Chemical Engineering Journal 160 (2010) 522–529

Contents lists available at ScienceDirect

Chemical Engineering Journal

journal homepage: www.elsevier.com/locate/cej

An integrated dynamic model for simulating a full-scale municipal wastewater treatment plant under fluctuating conditions

Fang Fang[a,b], Bing-Jie Ni[a], Wen-Ming Xie[a], Guo-Ping Sheng[a], Shao-Gen Liu[a], Zhong-Hua Tong[a], Han-Qing Yu[a,*]

[a] Department of Chemistry, University of Science & Technology of China, Hefei, 230026 China
[b] College of Environmental Science and Engineering, Hohai University, Nanjing, 210098, China

ARTICLE INFO

Article history:
Received 2 October 2009
Received in revised form 24 March 2010
Accepted 25 March 2010

Keywords:
Activated sludge model (ASM)
Genetic algorithm (GA)
Integrated model
Mechanistic model
Neural network (NN)
Wastewater treatment plant (WWTP)

ABSTRACT

In this study, an integrated dynamic model was developed through combining a mechanistic model, a neural network (NN) model and a genetic algorithm approach, in order to simulate the performance of a full-scale municipal wastewater treatment plant (WWTP) with substantial influent fluctuations. As the base of the integrated model, the mechanistic model was initially established based on the activated sludge model 3 and the EAWAG bio-P module, and was used to generate the residuals for the NN model. The NN model was employed to build the relationship between the input and output variables. The network weights of the NN model were optimized with a genetic algorithm approach. The resulting integrated model was applied to simulate the 5-month performance of a full-scale WWTP with significant influent fluctuations, and the simulation results matched the measured ones of the WWTP well even under influent disturbance conditions. Compared with the individual mechanistic model and NN model, the integrated model was able to capture sufficient residual information to compensate for the inaccuracy of the mechanistic model and improve the extrapolative capability of the NN model. This model established in our work is demonstrated to be an effective and useful tool to simulate the performance of WWTPs.

1. Introduction

Activated sludge processes are widely used for the treatment of both municipal and industrial wastewaters. One of main features of wastewater treatment plants (WWTPs) is the fluctuation of influent wastewater quality and quantity, e.g., high temporal variability of inflow and variable concentrations of components [1,2]. Thus, efficient modeling is essential to improve the monitoring, control and operation of WWTPs [3–5].

Activated sludge models (ASM1, 2, 2d, and 3) are able to simulate the complex physical, chemical and biological processes in WWTPs [3]. They have been proven to be the most effective tools to describe the removal processes of carbonaceous, nitrogenous and phosphate in WWTPs [6,7]. However, WWTPs are often characterized with a high daily variation in wastewater quality and/or quantity [5,8]. When a WWTP is subjected to such a variation, the ASM models may exhibit poor predict abilities, and there is a significant mismatch between the model predictions and the measured data [9]. Generally, these models are high-dimensional and contain a large number of kinetic and stoichiometric parameters, which should be determined with plant operation data [4,10]. In addition, the WWTP effluent is not often well predicted by the mechanistic models because of the separation problems of the secondary clarifiers in WWTPs. To sort out this problem, neural network (NN), an appropriate approach, should be introduced into the mechanistic models to improve their simulating capacity.

The NN approach is a powerful and effective tool to deal with problems to extract information out of complex, non-linear data without requiring prior knowledge of the relationships of the process parameters [9,11,12]. Because of its interpolative capability to capture the effects of some external disturbances, the NN approach has been successfully applied in multivariate non-linear bioprocesses as a useful tool to construct model [13–18]. However, the NN is typically used as a "black-box" approach, hiding the physics of the model process, and lacks for extrapolative capacity [9,19]. In addition, the gradient algorithm usually used in the back-propagation NN is a local search algorithm and may tend to fall into a local minimum and result in inconsistent and unpredictable performance [20]. Genetic algorithm (GA), based on the principles of survival of the fittest strategy, has been proven to be a powerful search and optimization method to solve problems with objective functions that are not continuous or differentiable [21,22]. Thus, an intro-

* Corresponding author. Tel.: +86 551 3607592; fax: +86 551 3601592.
E-mail address: hqyu@ustc.edu.cn (H.-Q. Yu).

1385-8947/$ – see front matter © 2010 Elsevier B.V. All rights reserved.
doi:10.1016/j.cej.2010.03.063

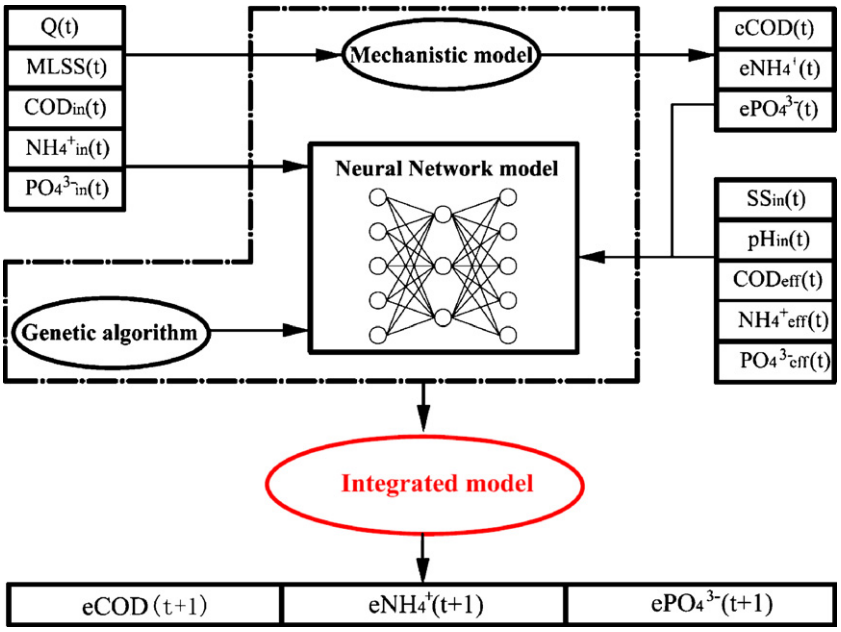

Fig. 1. Schematic diagram of the integrated model.

duction of GA might avoid trapping into the local minimum of NN. The NN-GA coupled models have been developed to optimize the various biological processes [18,23].

Therefore, in this study an integrated dynamic model was constructed and used to simulate the performance of WWTPs, especially under influent fluctuating conditions. Our work aimed at: (1) developing a mechanistic model based on ASM3 and EAWAG bio-P module to generate the residuals for the input of the NN; (2) using a back-propagation NN model to establish the relationship between the input and output variables to simulate the dynamic behavior of the WWTP; (3) introducing GA to optimize the NN weight vector; and (4) demonstrating the capacity of the integrated model with a full-scale WWTP as an example.

2. Model development

To simulate a full-scale WWTP, an integrated model consisted of a mechanistic model, a NN model and a GA approach was established. The mechanistic model was used as the base of the integrated model, and it generated the residuals for the NN model; NN was used to build the relationship between the input and output variables; the network weights of NN were optimized with the GA approach. The schematic representation of this integrated model is shown in Fig. 1.

The mechanistic model was established through a combination of the ASM3 [3] and the EAWAG bio-P module [24]. In the mechanistic model, the active biomass was divided into three categories: heterotrophic organisms (X_H), autotrophic organisms (X_A) and phosphorus accumulating organisms (X_{PAO}). The intracellular storage product by heterotrophic organisms (X_{STO}), and the cell-internal storage product (X_{PHA}) and polyphosphate (X_{PP}) by the phosphorous accumulating organisms were considered in the model. The inert particular organic material (X_I) arising from biomass endogenous respiration was also included.

Six dissolved chemical components were considered to be related to the biochemical processes and the reaction stoichiometry, e.g., dissolve oxygen (S_O), readily biodegradable substrate (S_S), ammonium-N (S_{NH_4}), nitrite and nitrate-N (S_{NO_x}), nitrogen gas (S_{N_2}) and inorganic soluble phosphors, primarily orthophosphate (S_{PO_4}). For the kinetic processes, hydrolysis process, in which all slowly biodegradable substrate contained in the influent became available to activated sludge, was considered. Eight processes for the heterotrophic organisms (X_H) and three processes for the autotrophic organisms (X_A) were included in the mechanistic model [3]. For the phosphorus accumulating organisms (X_{PAO}), eleven processes were taken into account [24]. The model was constructed in a matrix format. The kinetic processes of biological conversions adapted from ASM3 [3] and EAWAG bio-P [24] notation are outlined in Tables 1 and 2. The stoichiometrics of these processes are listed in Tables S1 and S2. The kinetic coefficients and initial parameters used in the model were adapted from the ASM3 and EAWAG bio-P module [3].

Influent flow rate $Q(t)$, mixed liquid volatile suspended solid (MLVSS) (t) and the influent concentrations of chemical oxygen demand [COD_{in} (t)], ammonium [$NH_{4,in}^{+}$ (t)] and phosphors [$PO_{4,in}^{3-}$ (t)] as input variables were put into the mechanistic model. As a result, the effluent concentrations of COD_{eff} (t), $NH_{4,eff}^{+}$ (t), $PO_{4,eff}^{3-}$ (t) were predicted. The residuals, $e(t)$ of COD, NH_4^+ and PO_4^{3-}, were defined as the differences between the measured data and predicted values by the mechanistic model.

The NN model was used to establish the relationship between the input and output variables. The feed-forward back-propagation NN, consisting of one input layer, one hidden layer and one output layer, was employed. Influent flow rate $Q(t)$; MLVSS(t) in the reactor; the influent concentrations of COD_{in} (t), $NH_{4,in}^{+}$ (t), $PO_{4,in}^{3-}$ (t), suspended solids [SS_{in} (t)], pH_{in} (t); the effluent concentrations of COD_{eff} (t), $NH_{4,eff}^{+}$ (t), $PO_{4,eff}^{3-}$ (t), SS_{eff} (t) were selected as the input variables of the NN model. Since dynamic information could be extracted from the residuals, the residuals $e(t)$ of COD, NH_4^+ and PO_4^{3-} generated from the mechanistic model were also put into the NN model as the input variables. The network outputs were the residuals $e(t+1)$ of COD, NH_4^+ and PO_4^{3-}. The number of the hidden neurons was determined from the learning curves, which were generated from the recall and generalization process through varying the number of neurons in the hidden layer [25]. The activation function of the neurons of both hidden and output layers were chosen as the sigmoid function, $f(x) = 1/(1 + e^{-x})$. Thus, this type of function allowed the network to learn non-linear relationships [26].

An "error back-propagation" algorithm was used as the NN learning algorithm, in which the input values of a sample were ini-

Table 1
Process kinetic rate equations for the mechanistic model.

Process	Process rate equation
1. Hydrolysis	$k_H \frac{X_S/X_H}{K_X+X_S/X_H} X_H$
Heterotrophic organisms (X_H)	
2. Aerobic storage	$k_{STO} \frac{S_S}{K_{H,S}+S_S} \frac{S_O}{K_{H,O}+S_O} X_H$
3. Anoxic storage	$k_{STO}\eta_{H,NO_x} \frac{S_S}{K_{H,S}+S_S} \frac{K_{H,O}}{K_{H,O}+S_O} \frac{S_{NO_x}}{K_{NO_x}+S_{NOX}} X_H$
4. Aerobic growth	$\mu_H \frac{X_{STO}/X_H}{K_{STO}+X_{STO}/X_H} \frac{K_{H,S}}{K_{H,S}+S_S} \frac{S_O}{K_{H,O}+S_O} \frac{S_{NH_4}}{K_{NH_4}+S_{NH_4}} \frac{S_{PO_4}}{K_{H,PO_4}+S_{PO_4}} X_H$
5. Anoxic growth	$\mu_H\eta_{H,NO_x} \frac{X_{STO}/X_H}{K_{STO}+X_{STO}/X_H} \frac{K_{H,S}}{K_{H,S}+S_S} \frac{K_{H,O}}{K_{H,O}+S_O} \frac{S_{NH_4}}{K_{NH_4}+S_{NH_4}} \frac{S_{NO_x}}{K_{NO_x}+S_{NO_x}} \frac{S_{PO_4}}{K_{H,PO_4}+S_{PO_4}} X_H$
6. Aerobic endogenous respiration	$b_{H,O} \frac{S_O}{K_{H,O}+S_O} X_H$
7. Anoxic endogenous respiration	$b_{H,NO_x} \frac{K_{H,O}}{K_{H,O}+S_O} \frac{S_{NO_x}}{K_{NO_x}+S_{NO_x}} X_H$
8. Aerobic respiration of X_{STO}	$b_{STO,O} \frac{S_O}{K_{H,O}+S_O} X_{STO}$
9. Anoxic respiration of X_{STO}	$b_{STO,NO_x} \frac{K_{H,O}}{K_{H,O}+S_O} \frac{S_{NO_x}}{K_{NO_x}+S_{NO_x}} X_{STO}$
Autotrophic organisms (X_A)	
10. Aerobic growth	$\mu_A \frac{S_O}{K_{A,O}+S_O} \frac{S_{NH_4}}{K_{A,NH_4}+S_{NH_4}} \frac{S_{PO_4}}{K_{A,PO_4}+S_{PO_4}} X_A$
11. Aerobic endogenous	$b_{A,O} \frac{S_O}{K_{A,O}+S_O} X_A$
12. Anoxic endogenous respiration	$b_{A,NO_x} \frac{K_{A,O}}{K_{A,O}+S_O} \frac{S_{NO_x}}{K_{A,NO_x}+S_{NO_x}} X_A$

tially applied to be learned as the inputs of the NN model. Then, the outputs of the NN model were compared with the given output values of the example and the errors were estimated. The errors were used to analyze which synaptic weight should be modified to reduce the errors for this sample, and the weights and the threshold values of the output and the hidden layers were adjusted using Eqs. (1)–(4):

$$w_{ij}^{t+1} = w_{ij}^{t} - \eta \frac{\partial E_k}{\partial x_j} y_i + \alpha(w_{ij}^{t} - w_{ij}^{t-1}) \quad (1)$$

$$\theta_j^{t+1} = \theta_j^{t} - \eta \frac{\partial E_k}{\partial x_j} + \alpha(\theta_j^{t} - \theta_j^{t-1}) \quad (2)$$

$$w_{hi}^{t+1} = w_{hi}^{t} - \eta \frac{\partial E_k}{\partial x_i} x_{k,h} + \alpha(w_{hi}^{t} - w_{hi}^{t-1}) \quad (3)$$

$$\theta_i^{t+1} = \theta_i^{t} - \eta \frac{\partial E_k}{\partial x_i} + \alpha(\theta_i^{t} - \theta_i^{t-1}) \quad (4)$$

where x_i, x_j, y_i and y_j are defined as the input and output values of the hidden layer and the output layer, respectively. w_{hi} is the connection weight from the hth neuron of the input layer to the ith neuron of the hidden layer, and w_{ij} is the connection weight from the ith neuron of the hidden layer to the jth neuron of the output layer. θ_i and θ_j are the threshold values of the hidden layer and output layer, respectively. η is the learning factor, and α is the momentum factor.

This procedure was repeated for each training example in the training set. The global error was calculated using the equation below:

$$E = \sum_{k=1}^{k} \sum_{j=1}^{j} \frac{(y_j - d_{k,j})^2}{2} \quad (5)$$

The computation process of the NN model would be terminated by two rules: (1) meeting the setting goal; and (2) reaching the maximum learning time.

The algorithm used in back-propagation is a gradient-descending algorithm. However, the gradient algorithm might tend to fall into a local minimum and result in inconsistent and unpre-

Table 2
Process kinetic rate equations for the mechanistic model (continuation).

Process	Process rate equation
Phosphorus accumulating organisms	
13. Storage of X_{PHA}	$q_{PHA} \frac{S_S}{K_{PAO,S}+S_S} \frac{X_{PP}/X_{PAO}}{K_{PAO,PP}+X_{PP}/X_{PAO}} X_{PAO}$
14. Aerobic storage of X_{PP}	$q_{PP} \frac{S_O}{K_{PAO,O}+S_O} \frac{S_{PO_4}}{K_{PP,PO_4}+S_{PO_4}} \frac{X_{PP}/X_{PAO}}{K_{PHA}+X_{PP}/X_{PAO}} \frac{K_{max,PAO}-X_{PP}/X_{PAO}}{K_{iPP,PAO}+K_{max,PAO}-X_{PP}/X_{PAO}} X_{PAO}$
15. Anoxic storage of X_{PP}	$q_{PP}\eta_{PAO,NOx} \frac{K_{PAO,O}}{K_{PAO,O}+S_O} \frac{S_{NO_x}}{K_{NO_x}+S_{NO_x}} \frac{S_{PO_4}}{K_{PP,PO_4}+S_{PO_4}} \frac{X_{PP}/X_{PAO}}{K_{PHA}+X_{PP}/X_{PAO}} \frac{K_{max,PAO}-X_{PP}/X_{PAO}}{K_{iPP,PAO}+K_{max,PAO}-X_{PP}/X_{PAO}} X_{PAO}$
16. Aerobic growth	$\mu_{PAO} \frac{S_O}{K_{PAO,O}+S_O} \frac{X_{PHA}/X_{PAO}}{K_{PHA}+X_{PHA}/X_{PAO}} \frac{S_{NH_4}}{K_{PAO,NH_4}+S_{NH_4}} \frac{S_{PO_4}}{K_{PAO,PO_4}+S_{PO_4}} X_{PAO}$
17. Anoxic growth	$\mu_{PAO}\eta_{PAO,NOx} \frac{K_{PAO,O}}{K_{PAO,O}+S_O} \frac{X_{PHA}/X_{PAO}}{K_{PHA}+X_{PHA}/X_{PAO}} \frac{S_{NO_x}}{K_{PAO,NO_x}+S_{NO_x}} \frac{S_{NH_4}}{K_{PAO,NH_4}+S_{NH_4}} \frac{S_{PO_4}}{K_{PAO,PO_4}+S_{PO_4}} X_{PAO}$
18. Aerobic endogenous respiration	$b_{PAO} \frac{S_O}{K_{PAO,O}+S_O} X_{PAO}$
19. Anoxic endogenous respiration	$b_{PAO}\eta_{PAO,NO_x} \frac{K_{PAO,O}}{K_{PAO,O}+S_O} \frac{S_{NO_x}}{K_{NO_x}+S_{NO_x}} X_{PAO}$
20. Aerobic respiration of X_{PP}	$b_{PP} \frac{S_O}{K_{PAO,O}+S_O} X_{PP}$
21. Anoxic respiration of X_{PP}	$b_{PP}\eta_{PAO,NO_x} \frac{K_{PAO,O}}{K_{PAO,O}+S_O} \frac{S_{NO_x}}{K_{NO_x}+S_{NO_x}} X_{PP}$
22. Aerobic respiration of X_{PHA}	$b_{PHA} \frac{S_O}{K_{PAO,O}+S_O} X_{PHA}$
23. Anoxic respiration of X_{PHA}	$b_{PHA}\eta_{PAO,NO_x} \frac{K_{PAO,O}}{K_{PAO,O}+S_O} \frac{S_{NO_x}}{K_{NO_x}+S_{NO_x}} X_{PHA}$

Table 3
Measured variables of the full-scale WWTP.

Variable	Symbol	Unit	Mean	Min–max
Influent COD	COD_{in}	mg/L	198	102–391
Influent NH_4^+	$NH_{4,in}^+$	mg/L	27.3	15.9–40.9
Influent PO_4^{3-}	$PO_{4,in}^{3-}$	mg/L	1.60	0.83–2.48
Influent SS	SS_{in}	mg/L	97	44–190
Influent pH	pH_{in}		7.41	6.89–7.74
Effluent COD	COD_{eff}	mg/L	40.8	21.6–58
Effluent NH_4^+	$NH_{4,eff}^+$	mg/L	3.0	0.1–10.1
Effluent PO_4^{3-}	$PO_{4,eff}^{3-}$	mg/L	1.31	0.44–2.17
Effluent SS	SS_{eff}	mg/L	11	5–19
MLVSS	MLVSS	mg/L	5774	3909–7983

dictable performance of the NN model [23]. Thus, to assure the good performance of the integrated model, GA, a global search algorithm, instead of local search algorithm, was introduced into the integrated model to search for the weight vector of the network (Fig. 1). The searching mechanisms of the integrated model are briefly described as follows:

(1) For the integrated model, the initial weights of NN were constructed based on training data sets.
(2) GA was employed to explore solutions among solution space. Once the GA generated a new solution, the NN model would be used to determine its fitness value for the GA to continue its searching process.
(3) After the stopping criterion, e.g., generation number, fitness threshold or population convergence, was met, the best solution would be generated by the GA.

After the best weight vectors of the network became available, they were introduced into the integrated model to simulate the WWTP performance.

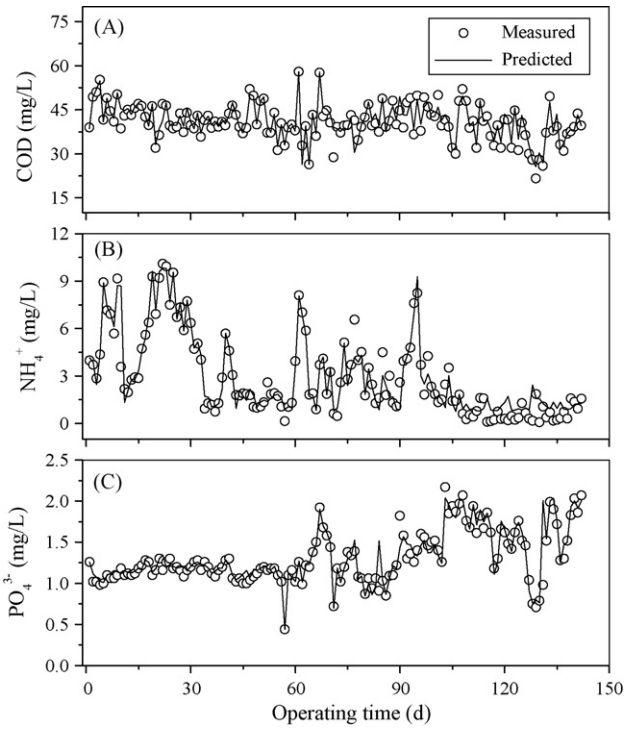

Fig. 2. Simulation results of the effluent COD, NH_4^+ and PO_4^{3-} concentrations using the integrated model.

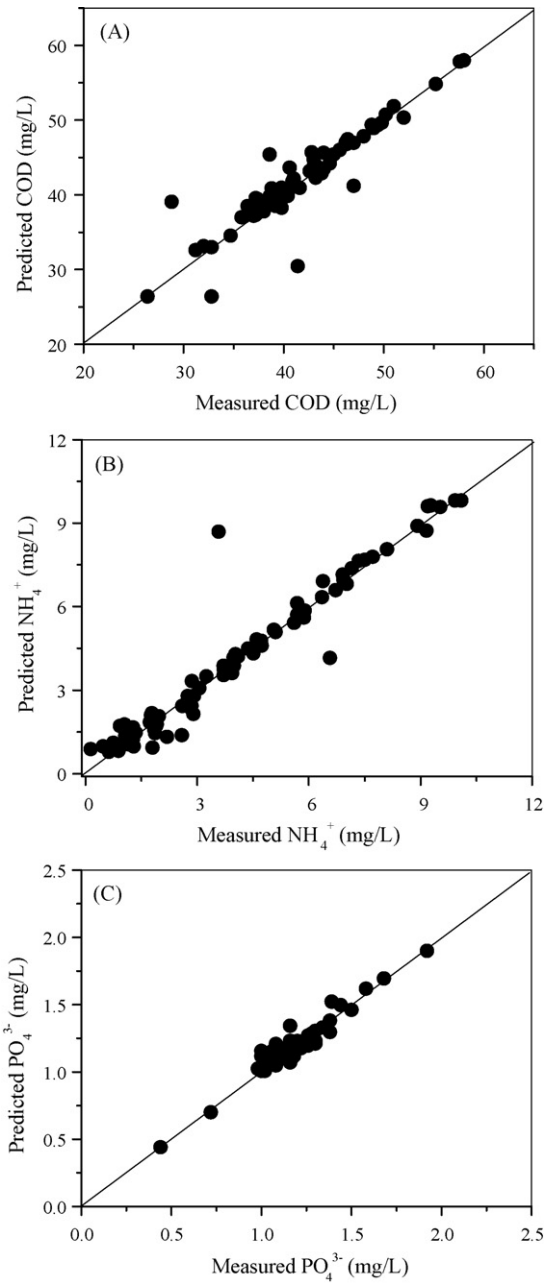

Fig. 3. Measured versus predicted values of (A) COD ($R^2 = 0.850$); (B) NH_4^+ ($R^2 = 0.930$); and (C) PO_4^{3-} ($R^2 = 0.926$) concentrations in the effluent with the integrated model for training data.

3. Materials and methods

3.1. Description of the Zhuzhuanjing WWTP

The WWTP is located in Hefei City, China, in which wastewater originating from the surrounding city areas is treated. The plant consists of gridirons, primary clarifiers, eight sequencing batch reactors (SBRs). Each SBR has a rectangle configuration and is operated in a fill-and-withdrawal mode. Wastewater is introduced and simultaneously mixed in the fill period; the reactor is aerated in the reaction period; later, the mixed liquor is allowed to settle in the settling period; at the end of each cycle the supernatant is discharged from the reactor. The working volume of each SBR is 2000 m^3. The time allotted for the operating cycle of each SBR is: 30 min for fill, 120 min for reaction, 60 min for settling, and 30 min

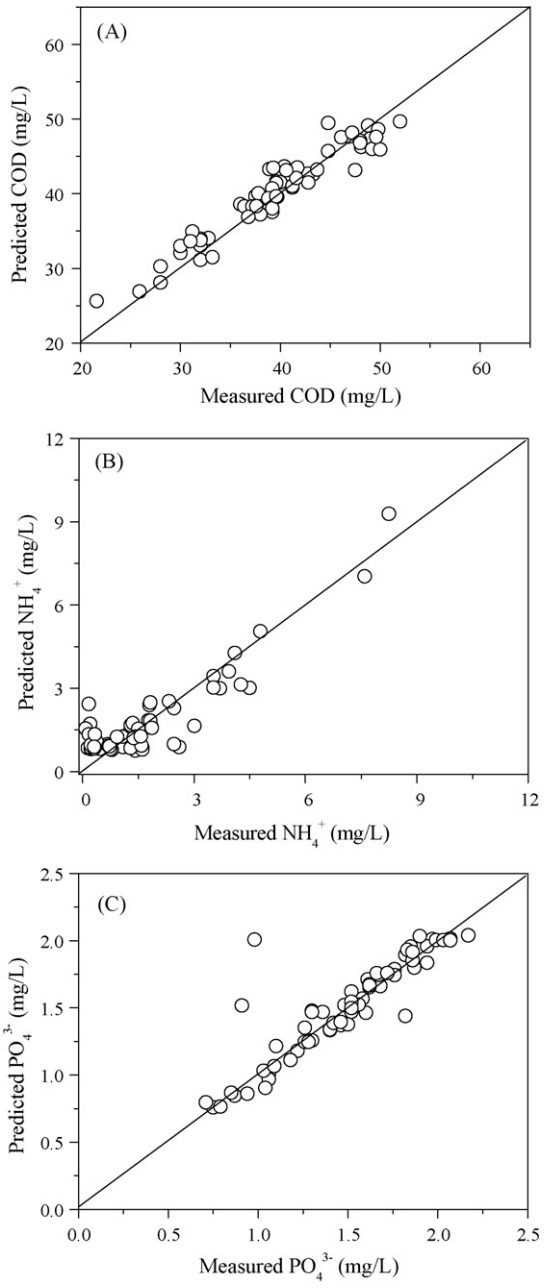

Fig. 4. Measured versus predicted values of: (A) COD (R^2 = 0.920); (B) NH_4^+ (R^2 = 0.792); and (C) PO_4^{3-} (R^2 = 0.794) concentrations in the effluent with the integrated model for testing data.

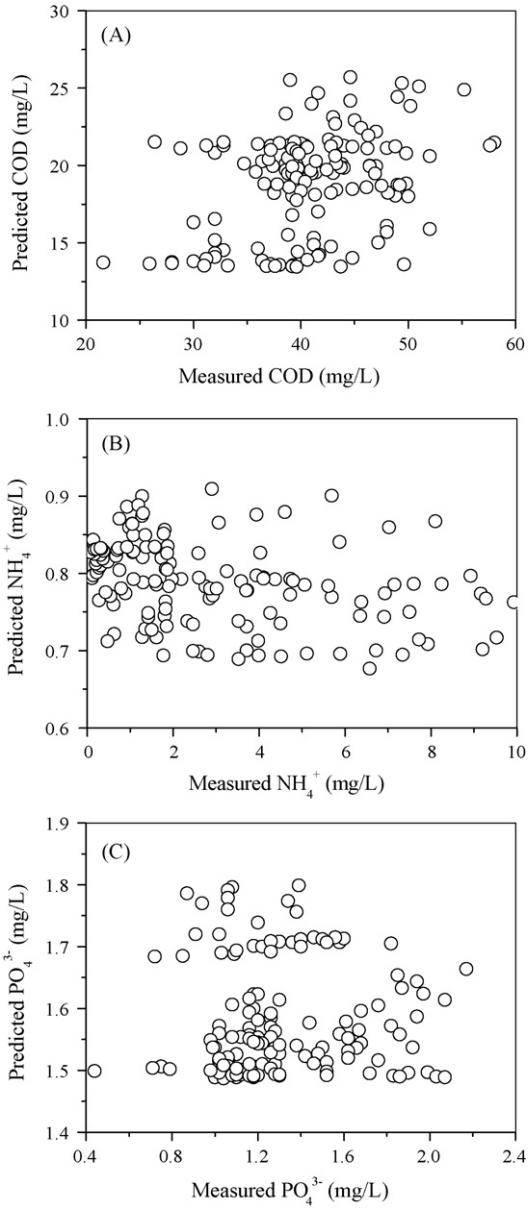

Fig. 5. Measured versus predicted values of: (A) COD (R^2 = 0.128), (B) NH_4^+ (R^2 = 0.128), and (C) PO_4^{3-} (R^2 = 0.001) concentrations in the effluent with the mechanistic model.

for decanting. The reactor effluent over a 5-month period was collected and measured almost every day (Fig. S1). Table 3 lists the available calculations from the plant along with their means, maximum and minimum values. An index, daily variation coefficient (K_{day}), was introduced to quantitatively evaluate the daily fluctuations of the wastewater quality, which is defined as follows [27]:

$$K_{day} = \frac{\text{maximum value of the wastewater quality}}{\text{average value of the wastewater quality}} \quad (6)$$

3.2. Wastewater characterization

Before the simulation with the mechanistic model, the organic matters in the municipal wastewater were fractionized to readily biodegradable organic compounds (S_S), inert soluble organic compounds (S_I), slowly biodegradable organic compounds (X_S) and inert particular organic compounds (X_I). The biodegradable COD in the influent was the sum of the S_S and X_S and was calculated from the formula proposed by Grady et al. [27]. The inert fraction S_I was determined independently and subtracted from the soluble COD to give the fraction S_S. S_I was evaluated from the effluent inert COD. The concentrations of X_S and X_I were estimated based on the biological oxygen demand (BOD_5) measurements [28].

The experimental data were directly put into the mechanistic model to generate the residuals. However, prior to the NN training, the data sets were normalized to the range of 0–1, in order to have the same order for the variables. After normalization, each variable had a zero of mean and a unitary variance according to its corresponding maximum and minimum values. In this way, the effect of different units was avoided and the variability was reduced. The data preprocessing above was carried out to ensure that the statistical distribution of the values for each net input and output was roughly uniform [25].

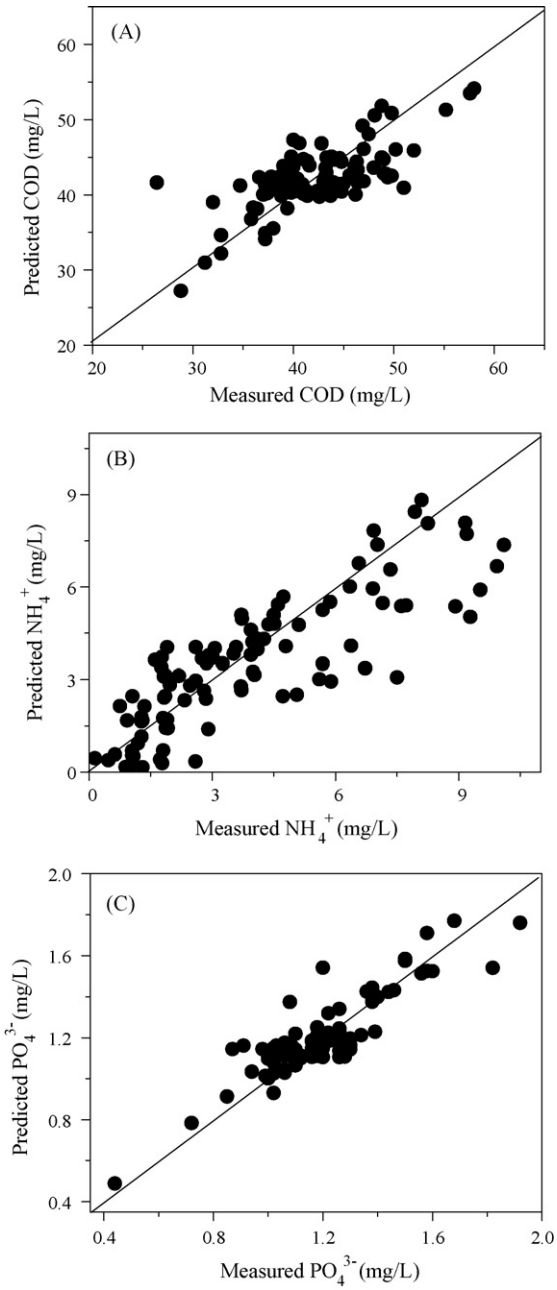

Fig. 6. Measured versus predicted values of: (A) COD ($R^2 = 0.517$), (B) NH_4^+ ($R^2 = 0.703$), and (C) PO_4^{3-} ($R^2 = 0.768$) concentrations in the effluent with the NN model for training data.

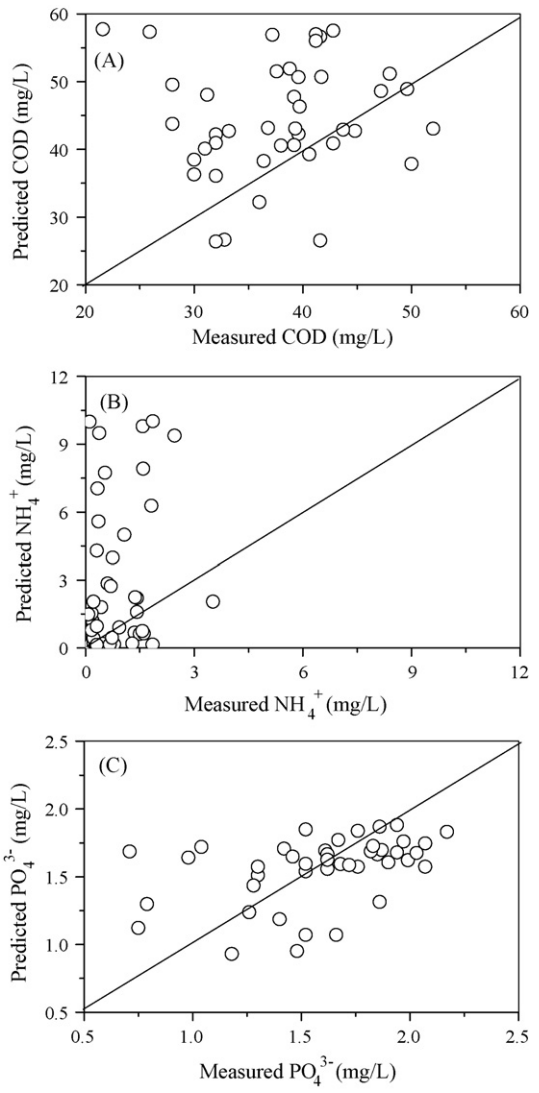

Fig. 7. Measured versus predicted values of: (A) COD ($R^2 = 0.010$), (B) NH_4^+ ($R^2 = 0.039$), and (C) PO_4^{3-} ($R^2 = 0.182$) concentrations in the effluent with the NN model for testing data.

3.3. Analysis and simulation

Measurements of COD, NH_4^+-N, NO_2^--N, NO^{3-}-N, PO_4^{3-}-P, pH, SS, MLSS and MLVSS followed the Standard Methods [29]. Simulation of the mechanistic model was performed with the AQUASIM software package [30]. For the NN model and integrated model, the computation was performed using software Matlab 7.0 (Mathworks, Natick, USA).

4. Results and discussion

4.1. Wastewater characterization

As shown in Fig. S1, the daily variations of influent COD, NH_4^+ and PO_4^{3-} concentrations are significant. The highest values of influent COD, NH_4^+ and PO_4^{3-} concentrations were detected to be 391, 41 and 2.5 mg/L, respectively, whereas their lowest values were only 102, 16 and 0.8 mg/L, respectively. Thus, the daily variation coefficients of COD, NH_4^+ and PO_4^{3-} are calculated as 1.97, 1.50 and 1.55, respectively. The high K_{day} values indicated that the fluctuation of wastewater quality of this WWTP was significant.

The fractions of S_S, S_I, X_S and X_I in the total influent COD in this WWTP were calculated. The S_S fraction in the influent was determined to be $30.1 \pm 3.9\%$ of the total COD, and the initial S_I fraction was estimated to be $10.3 \pm 2.3\%$ of the total COD. The initial established X_I fraction was approximately 11.0% of the total COD and the contribution of X_S was calculated to be 43.6% of the total COD.

4.2. Simulation results by the integrated model

Before generating the residuals by the mechanistic model, the parameter sensitivity analysis was performed through changing one by one in the simulation. The sensitivity analysis revealed that the maximum specific growth rates of X_H, X_A and X_{PAO} and the yield coefficients of X_H and X_A had great influences on the effluent COD, NH_4^+ and PO_4^{3-} concentrations. Therefore, the sensitive parameters were calibrated in AQUASIM [30]. Using the calibrated

Table 4
Root mean square errors for the training and testing data sets of the three models.

Model	Training	Testing
Mechanistic model	2.65	4.15
NN model	0.54	2.68
Integrated model	0.35	0.38

model, the residuals between the predicted and measured values were generated.

143 experimental samples were used for the integrated model simulation. The experimental samples were divided into different groups for training and testing sets. 60%, 70%, 80% and 90% of the samples were used for training the NN model, respectively. Correspondingly, 86, 100, 114 and 129 points were used for training, respectively. The remaining samples were used for testing. The root mean square error (RMSE) of the training and the testing sets of the above four groups had little difference (data not shown). Thus, in the subsequent study the former 100 samples were used for training or calibrating the NN model, whereas the remaining 43 samples were employed for model testing or verification.

The number of neurons of the hidden layer was an important parameter for the NN model. A low number of neurons does not provide sufficient parameters to train the neuronal network correctly. On the other hand, an excessive number of neurons leads to overtraining problems and its computational costs become higher [25]. Thus, the optimal number of the hidden neurons should be carefully selected. In this study, from the absolute errors (scaled) of both recall of the training data sets and the generalization of the testing data sets, the best network structure of 13 neurons in the hidden layer was determined (Fig. S2).

The simulation results with the integrated model illustrated in Fig. 2 show that the predicted effluent COD, NH_4^+ and PO_4^{3-} levels matched the measured ones well. The model was capable of accurately simulating the effects of the variation of influent COD loading. Satisfactory predictions of NH_4^+ and PO_4^{3-} were also observed with respect to the fluctuation of influent concentration. To better evaluate the simulation results, a line of unit slope has been drawn in both Figs. 3 and 4, in which a point situated exactly on the line indicates a perfect fit. Fig. 3 shows the comparison between the experimental values for the three output variables and the corresponding values obtained by fitting the integrated model of the training data sets. Comparison between the measured and predicted values for each output variable of the testing data sets is shown in Fig. 4. This figure shows that the trained integrated model showed no systematic over-prediction or under-prediction with regard to the output variables.

4.3. Comparison among the mechanistic model, the NN model and the integrated model

A comparison among the mechanistic model, the NN model and the integrated model was performed. The calibration results of the mechanistic model are illustrated in Fig. 5. Its low coefficient of determination (R^2) indicates that this model gave the poor prediction results, because some dynamics information was not taken into account in the mechanistic model. For instance, the poor separation in the secondary clarifiers had influence on the effluent quality, but this issue was not addressed in the mechanistic model. The simulation results of the NN model illustrated in Figs. 6 and 7 show that although this model could simulate the training data set well, it was over-trained and exhibited the poor extrapolative capacity. By contrast, the integrated model gave the best prediction results and was able to simulate the fluctuation of influent quality and quantity.

The RMSE is another index to evaluate the model performance. Table 4 lists the RMSE values of the training and testing data sets for the three models. The lowest RMSE value of the integrated model suggests that the integrated model gave the best prediction performance again.

The integrated model was capable of accurately simulating the full-scale WWTP performance under the variations of the influent loading and disturbances and describing the influence of separation process in the secondary clarifiers on the effluent quality. This indicates that the residuals contained sufficient relevant information about the dynamic behavior of the system, which could not be taken into account in the mechanistic model itself [9]. Such a simulation performance can be explained by the fact that the WWTP in this application was an inherently non-linear system with time-varying biological reactions and large influent variations. The integrated model was able to extract the non-linear information from the residuals to compensate for the inaccuracy of the mechanistic model and accordingly could improve the extrapolation ability of the NN model.

5. Conclusions

- In this work, an integrated dynamic model was established through combining a mechanistic model, an NN model and a GA approach to simulate the performance of a full-scale WWTP with substantial influent fluctuations.
- The mechanistic model was initially established based on the ASM 3 and the EAWAG bio-P module. It was used to generate the residuals for the NN model. The relationship between the input and output variables was built with the NN model, and the network weights of the NN model were optimized with a GA approach.
- The resulting integrated model was applied to simulate the 5-month performance of the WWTP. The simulation results shows that the predicted values by the integrated model matched the measured ones of the plant well under influent disturbance conditions.
- Compared with the mechanistic model and the NN model, the integrated model was able to capture sufficient residual information to compensate for the inaccuracy of the mechanistic model and improve the extrapolative capability of the NN model.
- Considering the great variations in the influent and high disturbances of WWTPs, the integrated model established in our work is an effective and useful tool to simulate such a complex biological system like WWTPs.

Acknowledgements

The authors wish to thank the Natural Science Foundation of China (50625825 and 50738006), the Key Special Program on the S&T for the Pollution Control (2008ZX07316-002 and 2008ZX07010-005) the Natural Science Foundation of Hohai University (2009422811) and the Anhui R&D Key Project (07010301022 and 08010302109) for the partial support of this study.

Appendix A. Supplementary data

Supplementary data associated with this article can be found, in the online version, at doi:10.1016/j.cej.2010.03.063.

References

[1] Metcalf & Eddy, Inc., Wastewater Engineering: Treatment, Disposal and Reuse, 2nd ed., 1978.
[2] G.M. Zeng, Y.P. Lin, X.S. Qin, G.H. Huang, J.B. Li, R. Jiang, Optimum municipal wastewater treatment plant design with consideration of uncertainty, J. Environ. Sci. 16 (2004) 126–131.

[3] M. Henze, W. Gujer, T. Mino, M.C.M. van Loosdrecht, Activated sludge models ASM1, ASM2, ASM2d, and ASM3. IWA Scientific and technical report no. 9, IWA Publishing, London, UK, 2009.
[4] C.K. Yoo, P.A. Vanrolleghem, I.B. Lee, Nonlinear modeling and adaptive monitoring with fuzzy and multivariate statistical methods in biological wastewater treatment plants, J. Biotechnol. 105 (2003) 135–163.
[5] B.J. Ni, W.M. Xie, S.G. Liu, H.Q. Yu, Y.Z. Wang, G. Wang, X.L. Dai, Modeling and simulation of the sequencing batch reactor at a full-scale municipal wastewater treatment plant, AIChE J. 55 (2009) 2186–2196.
[6] K.V. Gernaey, M.C.M. van Loosdrecht, M. Henze, M. Lind, S.B. Jorgensen, Activated sludge wastewater treatment plant modelling and simulation: state of the art, Environ. Model. Softw. 19 (2004) 763–783.
[7] A. Vandekerckhove, W. Moerman, S.W.H. Hulle, Full-scale modeling of a food industry wastewater treatment plant in view of process upgrade, Chem. Eng. J. 135 (2008) 185–194.
[8] M.M. Wu, R.F. Hickey, Dynamic model for UASB reactor including reactor hydraulics, reaction, and diffusion, J. Environ. Eng. ASCE 123 (1997) 244–252.
[9] D.S. Lee, C.O. Jeon, J.M. Park, K.S. Chang, Hybrid neural network modeling of a full-scale industrial wastewater treatment process, Biotechnol. Bioeng. 78 (2002) 670–682.
[10] F. Fang, B.J. Ni, H.Q. Yu, Estimating the kinetic parameters of activated sludge storage using weighted nonlinear least-squares and accelerating genetic algorithm, Water Res. 43 (2009) 2595–2604.
[11] K.V. Kumar, K. Porkodi, Modelling the solid-liquid adsorption processes using artificial neural networks trained by pseudo second order kinetics, Chem. Eng. J. 148 (2009) 20–25.
[12] J.S. Torrecilla, M.L. Mena, P. Yanez-Sedeno, J. Garcia, Field determination of phenolic compounds in olive oil mill wastewater by artificial neural network, Biochem. Eng. J. 38 (2008) 171–179.
[13] I.D.S. Henriques, D.S. Aga, P. Mendes, S.K. O'Connor, N.G. Love, Metabolic footprinting: A new approach to identify physiological changes in complex microbial communities upon exposure to toxic chemicals, Environ. Sci. Technol. 41 (2007) 3945–3951.
[14] Y.S.T. Hong, M.R. Rosen, R. Bhamidimarri, Analysis of a municipal wastewater treatment plant using a neural network-based pattern analysis, Water Res. 37 (2003) 1608–1618.
[15] Y.H. Kim, C.K. Yoo, I.B. L, Optimization of biological nutrient removal in a SBR using simulation-based iterative dynamic programming, Chem. Eng. J. 139 (2008) 11–19.
[16] B. Raduly, K.V. Gernaey, A.G. Capodaglio, P.S. Mikkelsen, M. Henze, Artificial neural networks for rapid WWTP performance evaluation: methodology and case study, Environ. Model. Softw. 22 (2007) 1208–1216.
[17] M. Rajendra, P.C. Jen, H. Raheman, Prediction of optimized pretreatment process parameters for biodiesel production using ANN and GA, Fuel 88 (2009) 868–875.
[18] J.L. Wang, W. Wan, Optimization of fermentative hydrogen production process using genetic algorithm based on neural network and response surface methodology, Int. J. Hydrogen Energy 34 (2009) 255–261.
[19] C.S. Akratos, J.N.E. Papaspyros, V.A. Tsihrintzis, An artificial neural network model and design equations for BOD and COD removal prediction in horizontal subsurface flow constructed wetlands, Chem. Eng. J. 143 (2008) 96–110.
[20] R.S. Sexton, R.E. Dorsey, J.D. Johnson, Toward global optimization of neural networks: a comparison of the genetic algorithm and back propagation, Decis. Support Syst. 22 (1998) 171–185.
[21] J. Holland, Adaptation in Natural and Artificial Systems, University of Michigan Press, Ann Arbor, MI, 1975.
[22] M.C.A.F. Rezende, C.B.B. Costa, A.C. Costa, M.R.W. Maciel, R.M. Filho, Optimization of a large scale industrial reactor by genetic algorithms, Chem. Eng. Sci. 63 (2008) 330–341.
[23] A.C.P. Filho, R.M. Filho, Hybrid training approach for artificial neural networks using genetic algorithms for rate of reaction estimation: application to industrial methanol oxidation to formaldehyde on silver catalyst, Chem. Eng. J. 157 (2010) 501–508.
[24] L. Rieger, G. Koch, M. Kuhni, W. Gujer, H. Siegrist, The EAWAG Bio-P module for activated sludge model no. 3, Water Res. 35 (2001) 3887–3903.
[25] F.S. Mjalli, S. Al-Asheh, H.E. Alfadala, Use of artificial neural network black-box modeling for the prediction of wastewater treatment plants performance, J. Environ. Manage. 83 (2007) 329–338.
[26] I. Machon, H. Lopez, J. Rodriguez-Iglesias, E. Maranon, I. Vazquez, Simulation of a coke wastewater nitrification process using a feed-forward neuronal net, Environ. Model. Softw. 22 (2007) 1382–1387.
[27] C.P.L. Grady Jr., G.T. Daigger, H.C. Lim, Biological Wastewater Treatment, 2nd ed., Marcel Dekker, New York, 1999.
[28] J. Makinia, K.H. Rosenwinkel, V. Spering, Long-term simulation of the activated sludge process at the Hanover-Gummerwald pilot WWTP, Water Res. 39 (2005) 1489–1502.
[29] APHA, Standard Methods for the Examination of Water and Wastewater, 19th ed., American Public Health Association, Washington, DC, 1995.
[30] P. Reichert, Aquasim 2. 0-User Manual. Computer Program for the Identification and Simulation of Aquatic Systems, EAWAG, Dübendorf, Switzerland, 1998.